O^6-Ethylguanine Carcinogenic Lesions in DNA: An NMR Study of O^{6}etG·C Pairing in Dodecanucleotide Duplexes†

Matthew W. Kalnik,‡ Benjamin F. L. Li,§ Peter F. Swann,§ and Dinshaw J. Patel*,‡

Department of Biochemistry and Molecular Biophysics, College of Physicians and Surgeons, Columbia University, New York, New York 10032, and Biochemistry Department, University College London, London WC1E 6BT, England

Received January 20, 1989

ABSTRACT: The pairing of O^{6}etG with C located four base pairs in from either end of the self-complementary d(C1-G2-C3-O^{6}etG4-A5-G6-C7-T8-C9-G10-C11-G12) duplex (designated O^{6}etG·C 12-mer) has been investigated from an analysis of proton and phosphorus two-dimensional NMR experiments. The structural consequences of increasing the alkyl group size were elucidated from a comparative study of the pairing of O^{6}meG4 with C9 in a related sequence (designated O^{6}meG·C 12-mer). The NMR parameters for both O^{6}alkG-containing dodecanucleotides are also compared with those of the control sequence containing G4·C9 base pairs (designated G·C 12-mer). The NOE cross-peaks detected in the two-dimensional NOESY spectra of the O^{6}alkG·C 12-mer duplexes in H_2O solution establish that the O^{6}etG4/O^{6}meG4 and C9 bases at the lesion site stack into the helix between the flanking C3·G10 and A5·T8 Watson–Crick base pairs. The amino protons of C9 at the O^{6}alkG4·C9 lesion site resonate as an average resonance at 7.78 and 7.63 ppm in the O^{6}etG·C 12-mer and O^{6}meG·C 12-mer duplexes, respectively. The observed NOEs between the amino protons of C9 and the CH_3 protons of O^{6}alkG4 establish a syn orientation of the O^6-alkyl group with respect to the N^1 of alkylated guanine. A wobble alignment of the O^{6}alkG4·C9 base pair stablized by two hydrogen bonds, one between the amino group of C9 and N^1 of O^{6}alkG and the other between the amino group of O^{6}alkG and N^3 of C9, is tentatively proposed on the basis of the NOEs between the amino protons of C9 at the lesion site and the imino protons of flanking Watson–Crick base pairs. The proton and phosphorus chemical shift differences between the O^{6}etG·C 12-mer and O^{6}meG·C 12-mer duplexes are small compared to the differences between these O^{6}alkG-containing duplexes and the control G·C 12-mer duplex.

Carcinogenic nitrosamines form alkylating agents during metabolism in mammals. These metabolites can modify the exocyclic oxygen groups of DNA bases (Singer, 1979; Pegg, 1983). The O^6-alkylguanine lesion has been the focus of much research and has been demonstrated to introduce G·C → A·T transitions in vitro and in vivo (Abbott & Saffhill, 1979; Gerchman & Ludlum, 1973; Loechler et al., 1984). These transitions are the predominant mutations found in eukaryotes after exposure to *N*-nitroso compounds (Coulondre & Miller, 1977; Richardson et al., 1987). The carcinogenic and mutagenic potential of *N*-nitroso compounds may be linked to the formation of O^{6}meG since *N*-methyl-*N*-nitrosourea-induced mammary tumors exhibit G·C → A·T transitions in the H-ras-1 oncogene (Zarbl et al., 1985).

One of the mechanisms proposed for these nitrosamine-induced transition mutations is the preferential base pairing of O^{6}alkG with thymine during replication (Abbott & Saffhill, 1979; Parthasarathy & Fridey, 1986; Yamagata et al., 1988). Understanding the structure of the O^{6}alkG base pair with cytosine may explain why the polymerase does not accept the O^{6}alkG·C base pair. The base pairing of O^{6}alkG·C may also reveal the structural features recognized by the repair enzyme, O^6-alkylguanine-DNA alkyltransferase.

Ethylation and higher order alkylations at position 6 of guanine have gained an important role in theories of alkylation leading to mutagenesis and carcinogenesis. The cellular O^6-alkylguanine-DNA alkyltransferases are inefficient at removing the O^{6}etG adduct (Pegg, 1977; Lindahl, 1982; Pegg, 1984; Singer, 1985), thereby prolonging the lifetime of this potentially mutagenic adduct.

Chart I

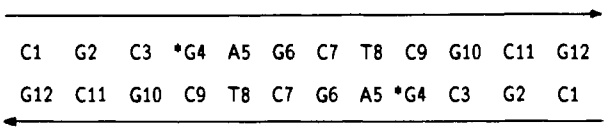

*G4 = G
= O^{6}meG
= O^{6}etG

Three self-complementary dodecanucleotide duplexes, d-(C1-G2-C3-*G4-A5-G6-C7-T8-C9-G10-C11-G12) containing a G·C (designated G·C 12-mer), a O^{6}meG·C (designated O^{6}meG·C 12-mer), or a O^{6}etG·C (designated O^{6}etG·C 12-mer) base pair at the fourth base pair in from either end of the helix (see Chart I), are the focus of this two-dimensional NMR study.

Experimental Procedures

NMR Sample Preparation. The NMR spectra for the G·C 12-mer, O^{6}meG·C 12-mer, and O^{6}etG·C 12-mer duplexes were recorded in 0.1 M NaCl, 10 mM phosphate, and 1 mM EDTA aqueous buffer. The concentration of the G·C 12-mer and O^{6}etG·C 12-mer duplexes was 400 A_{260} units in 0.35 mL, while the concentration of the O^{6}meG·C 12-mer duplex was 370 A_{260}

† This research was supported by NIH GM 34504 to D.J.P. and grants from the Cancer Research Campaign and the Medical Research Council to P.F.S. NMR studies were conducted on instruments purchased with funds provided by the Robert Woods Johnson, Jr. Charitable Trust and the Matheson Foundation.

‡ Columbia University.
§ University College London.

0006-2960/89/0428-6182$01.50/0

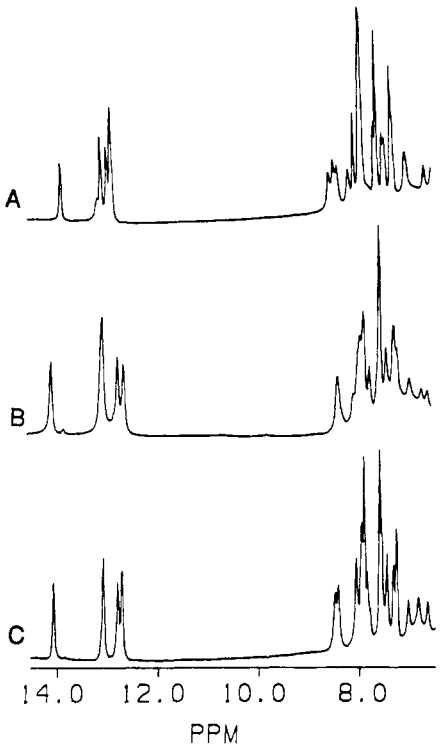

FIGURE 1: The 500-MHz proton NMR spectrum (6.5–15.0 ppm) of (A) the G·C 12-mer duplex in 0.1 M NaCl, 10 mM phosphate, and H_2O, pH 6.4 at 15 °C, (B) the O⁶meG·C 12-mer duplex in 0.1 M NaCl, 10 mM phosphate, and H_2O, pH 6.35 at 15 °C, and (C) the O⁶etG·C 12-mer duplex in 0.1 M NaCl, 10 mM phosphate, and H_2O, pH 6.35 at 15 °C.

units in 0.35 mL. The pH values quoted in D_2O solution are uncorrected pH meter readings.

NMR Experiments. The procedures for one- and two-dimensional NMR data collection on DNA oligomers in H_2O and D_2O solution and data processing are outlined in the preceding paper (Kalnik et al., 1989).

Results

The numbering system for the parent G·C 12-mer, O⁶meG·C 12-mer, and O⁶etG·C duplexes is outlined in Chart I.

Exchangeable Proton Spectra. The one-dimensional exchangeable proton NMR spectra (6.5–15.0 ppm) of the G·C 12-mer (pH 6.40), O⁶meG·C 12-mer (pH 6.35), and O⁶etG·C 12-mer (pH 6.60) duplexes in H_2O, at 5 °C, are presented in panels A–C of Figure 1, respectively. The spectra display similar patterns in the imino (12.5–14.2 ppm) and the non-exchangeable aromatic and amino proton (6.5–8.5 ppm) regions (Figure 1). The self-complementary G·C 12-mer duplex exhibits six partially resolved imino protons corresponding to the single A·T and five G·C base pairs. The O⁶meG·C 12-mer and O⁶etG·C 12-mer self-complementary duplexes exhibit only five partially resolved imino protons since the alkylation at the O⁶ of residue G4 alters the bonding pattern in the purine ring, causing deprotonation at the N^1 position.

Expanded contour plots of the phase-sensitive NOESY spectrum (120-ms mixing time) of the O⁶etG·C 12-mer duplex in H_2O, pH 6.35 at 5 °C, are plotted in Figure 2. The NOESY cross-peak assignments of the O⁶etG·C 12-mer duplex are outlined in the caption to Figure 2 and follow the procedures presented in the preceding paper on the O⁶etG·T 12-mer duplex (Kalnik et al., 1989).

The hydrogen-bonded and exposed cytosine amino protons of Watson–Crick G·C base pairs are observed as distinct

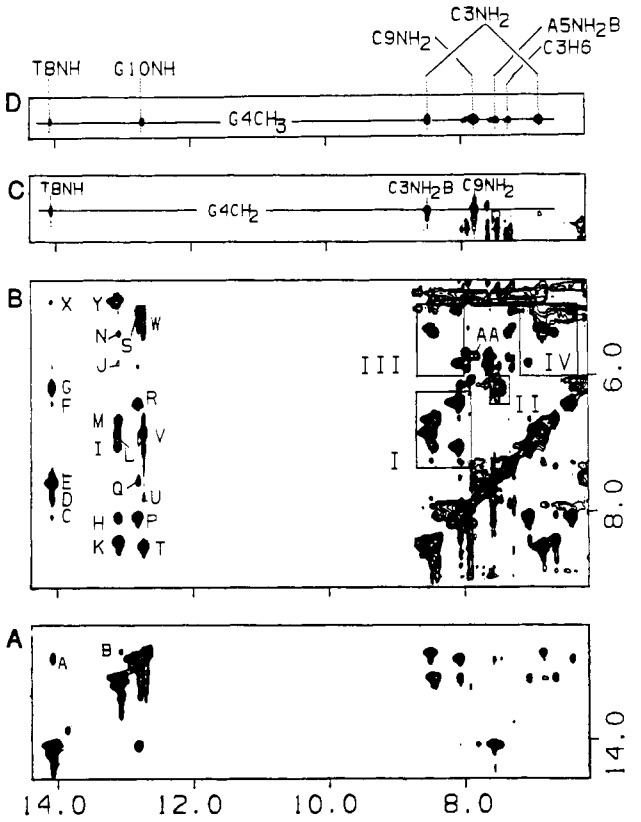

FIGURE 2: Phase-sensitive NOESY (120-ms mixing time) spectrum of the O⁶etG·C 12-mer duplex in 0.1 M NaCl, 10 mM phosphate, and H_2O, pH 6.10 at 5 °C. (A) Cross-peaks establishing connectivities between imino protons in the symmetrical 12.0–14.5-ppm spectral range. (B) Cross-peaks establishing connectivities between the imino and amino protons (5.0–14.5 ppm) and the base and amino protons (7.2–8.5 ppm). (C) Cross-peaks establishing the connectivities between the CH_2 protons of O⁶etG4 (3.0–4.2 ppm) and the exchangeable imino and amino protons (5.0–14.5 ppm). (D) Cross-peaks establishing connectivities between the CH_3 protons of O⁶etG4 (0.8–1.3 ppm) and the exchangeable imino and amino protons (5.0–14.5 ppm). Cross-peaks A–Y are assigned as follows: The 14.06-ppm imino proton of T8 develops NOEs to the imino proton of G6 (peak A), to the hydrogen-bonded (peak C) and exposed (peak F) amino protons of C7, to the H2 (peak E) and the hydrogen-bonded (peak E) and exposed (peak G) amino protons of A5, and to the hydrogen-bonded and exposed amino protons of C9 (peak D). The 13.09-ppm imino proton of G12 develops NOEs to the hydrogen-bonded (peak H) and exposed (peak I) and H5 (peak J) protons of C1. The 13.08-ppm imino proton of G2 develops NOEs to the imino proton of G10 (peak B), to the hydrogen-bonded (peak K) and exposed (peak M) amino and H5 (peak N) protons of C11, and to the hydrogen-bonded (peak K) and exposed (peak L) amino protons of C3. The 12.78-ppm imino proton of G6 exhibits NOEs to the hydrogen-bonded (peak P) and exposed (peak R) amino and H5 (peak S) protons of C7 and to the H2 proton of A5 (peak Q). The 12.72-ppm imino proton of G10 develops NOEs to the hydrogen-bonded (peak T) and exposed (peak V) amino and H5 (peak W) protons to C3 and to the hydrogen-bonded and exposed amino protons of C9 (peak U). Cross-peak AA is identified as the NOE between the amino and H5 protons of C9. Cross-peaks X and Y are chemical exchange cross-peaks between the solvent H_2O and the imino protons of T8, G12, and G2. Boxed region I outlines the NOE cross-peaks between the hydrogen-bonded and exposed cytosine amino protons within the same base pair. Boxed region II outlines the NOE cross-peaks between the hydrogen-bonded and exposed adenine amino protons. Boxed regions III and IV outline the NOE cross-peaks between the cytosine H5 protons and the hydrogen-bonded and exposed amino protons within the same base pair.

resonances separated by ~1.5 ppm in DNA oligomer duplexes. By contrast, the hydrogen-bonded and exposed amino protons of C9 at the O⁶et G4·C9 lesion site resonate as an average resonance at 7.78 ppm in the O⁶etG·C 12-mer duplex. The superimposed resonances of the amino protons of C9 are identified by their NOEs to the H5 of C9 (peak AA, Figure

Table I: Proton Chemical Shifts in the O⁶etG·C 12-mer Duplex

	chemical shifts (ppm)[a]								
base pair	T-H3		G-H1	C-H4b	C-H4e	A-H6b		A-H6e	A-H2
C1·G12			13.09	8.08	7.00				
G2·C11			13.08	8.43	6.64				
C3·G10			12.72	8.49	6.82				
O⁶etG4·C9				7.78	7.78				
A5·T8	14.06					7.50		6.18	7.59
G6·C7			12.78	8.07	6.40				
	chemical shifts (ppm)[b]								
base	H8	H2	H6	H5/CH3	H1′	H2′	H2″	H3′	H4′
C1			7.61	5.85	5.73	1.98	2.40	4.66	4.05
G2	7.94				5.93	2.62	2.75	4.97	4.34
C3			7.27	5.33	5.47	1.60	2.04	4.75	4.12
O⁶etG4	7.98				5.65	2.75	2.81	5.00	4.33
A5	7.98	7.59			5.96	2.60	2.77	5.01	4.41
G6	7.63				5.81	2.52	2.61	4.92	4.39
C7			7.30	5.11	5.91	2.02	2.50	4.70	4.20
T8			7.48	1.58	5.90	2.27	2.35	4.88	4.20
C9			7.55	5.69	6.12	2.16	2.59	4.88	4.25
G10	7.84				5.77	2.55	2.63	4.95	4.31
C11			7.36	5.42	5.83	1.90	2.35	4.85	4.17
G12	7.92				6.12	2.37	2.59	4.64	4.15

[a] 0.1 M NaCl, 10 mM phosphate, H_2O, pH 6.9, 5 °C; exchangeable protons. [b] 0.1 M NaCl, 10 mM phosphate, D_2O, pH 6.35, 25 °C; nonexchangeable protons.

2B) and to the imino protons of the flanking A5·T8 (peak D, Figure 2B) and C3·G10 (peak U, Figure 2B) base pairs in the O⁶etG·C 12-mer duplex. The imino proton, cytosine and adenine amino proton, and adenine H2 proton chemical shifts of the O⁶etG·C 12-mer duplex at 5 °C are listed in the upper part of Table I.

Several NOEs are detected involving the $O^6CH_2CH_3$ protons of O⁶etG at the O⁶etG4·C9 lesion site. The CH_3 protons of the O⁶etG group exhibit NOEs to the superimposed amino protons of the C9 residue across the base pair, to the thymine imino and the hydrogen-bonded adenine amino protons of the flanking A5·T8 base pair, and to the guanine imino and the hydrogen-bonded and exposed cytosine amino protons of the flanking C3·G10 base pair (Figure 2D). The CH_2 protons of the O⁶etG group exhibit fewer NOEs within the (C3-O⁶etG4-A5)·(T8-C9-G10) segment and are limited to the amino protons of C9, the imino proton of T8, and the hydrogen-bonded amino proton of C3 (Figure 2C).

Expanded contour plots of the phase-sensitive NOESY spectrum (120-ms mixing time) of the O⁶meG·C 12-mer duplex in H_2O, pH 6.35 at 5 °C, are plotted in Figure 3. The cross-peak assignments are listed in the caption to Figure 3. Striking similarities exist in the cross-peak patterns observed in the NOESY spectra of the O⁶etG·C 12-mer (Figure 2A,B) and the O⁶meG·C 12-mer (Figure 3A,B) duplexes. A few percent of the G·C 12-mer duplex is present in the O⁶meG·C 12-mer duplex sample, and additional cross-peaks from this minor component (designated by asterisks) are observed in the NOESY spectrum of the O⁶meG·C 12-mer duplex (Figure 3A,B).

The O⁶meG·C 12-mer duplex was labeled with ^{13}C at the O^6CH_3 group of the O⁶meG4. Hence, the O^6CH_3 proton resonance is split into a doublet by the two-bond ^1H–^{13}C scalar coupling. The CH_3 proton doublet of O⁶meG4 develops NOEs to the amino protons of C9, to the imino protons of T8 and G10, and to the hydrogen-bonded and exposed amino protons of C3 in the (C3-O⁶meG4-A5)·(T8-C9-G10) segment (Figure 3C). Additional distance connectivities between the O⁶meG4·C9 lesion pair and flanking C3·G10 and A5·T8 base pairs are observed between the amino protons of C9 and the imino protons of T8 (peak D, Figure 3B) and G10 (peak U, Figure 3B). The corresponding exchangeable proton chemical shifts of the O⁶meG·C 12-mer are listed in the upper part of Table II.

The phase-sensitive NOESY spectrum (120-ms mixing time) of the G·C 12-mer duplex in H_2O, pH 6.40 at 5 °C (Figure 4), exhibits similar cross-peak patterns as observed for the unmodified base pairs in the O⁶etG·C 12-mer duplex (Figure 2) and the O⁶meG·C 12-mer duplex (Figure 3). The most obvious differences are the presence of the imino proton of G4 (12.85 ppm) and the observation of separate resonances for the hydrogen-bonded (8.53 ppm) and exposed (6.99 ppm) amino protons of C9. The NOESY cross-peak assignments are outlined in the caption of Figure 4. The chemical shifts of the exchangeable imino and amino proton and the nonexchangeable adenine H2 proton resonances in the G·C 12-mer duplex at 5 °C are given in the upper part of Table III.

Nonexchangeable Proton Assignments. Nonexchangeable protons in DNA can be assigned by two-dimensional through-bond COSY and through-space NOESY experiments in D_2O. Expanded regions of the NOESY spectrum (250-ms mixing time) of the O⁶etG·C 12-mer at 25 °C, in D_2O, pH 6.90, establishing distance connectivities between the base protons (7.2–8.0 ppm) and the sugar H1′ and cytosine H5 protons (5.0–6.2 ppm) and the thymine CH_3 protons (1.5–1.8 ppm) are plotted in panels A and B of Figure 5, respectively. The distance connectivities for the purine H8 and the pyrimidine H6 protons to their own and 5′-flanking sugar H1′ protons can be traced along the helix from residue C1 to residue G12 without interruption at the O⁶etG4·C9 lesion site in the O⁶etG·C 12-mer duplex. Additional cross-peaks reflect distance connectivities between base protons in purine H8-pyrimidine H6(3′–5′)pyrimidine H5/CH_3 steps and between adjacent adenine H2 and sugar H1′ protons on the same and partner strand (assignments listed in the caption to Figure 5).

The corresponding expanded regions of the NOESY spectrum (250-ms mixing time) of the O⁶meG·C 12-mer duplex in D_2O sample buffer, pH 6.35, and of the G·C 12-mer duplex, pH 6.4, are plotted in Figures 6 and 7, respectively.

Analysis of the COSY spectrum, where the H1′, H2′,2″, H3′, and H4′ protons are identified by virtue of their three-bond couplings, in conjunction with analysis of other NOESY

Table II: Proton Chemical Shifts in the O⁶meG·C 12-mer Duplex

	chemical shifts (ppm)[a]						
base pair	T-H3	G-H1	C-H4b	C-H4e	A-H6b	A-H6e	A-H2
C1·G12		13.03	8.08	7.02			
G2·C11		13.04	8.45	6.66			
C3·G10		12.62	8.38	6.74			
O⁶meG4·C9			7.63	7.63			
A5·T8	14.01				7.40	6.13	7.58
G6·C7		12.71	8.04	6.43			

	chemical shifts (ppm)[b]								
base	H8	H2	H6	H5/CH3	H1′	H2′	H2″	H3′	H4′
C1			7.61	5.85	5.71	1.96	2.39	4.66	4.05
G2	7.93				5.90	2.61	2.71	4.95	4.32
C3			7.23	5.33	5.57	1.63	2.16	4.75	4.11
O⁶meG4	7.98				5.60	2.61	2.71	4.99	4.29
A5	7.96	7.61			5.98	2.58	2.77	5.00	4.39
G6	7.58				5.75	2.49	2.59	4.90	4.35
C7			7.30	5.10	5.87	2.03	2.49	4.68	4.19
T8			7.47	1.55	5.92	2.22	2.40	4.86	4.15
C9			7.59	5.69	6.07	2.15	2.57	4.84	4.23
G10	7.79				5.78	2.50	2.60	4.91	4.29
C11			7.33	5.39	5.79	1.89	2.33	4.80	4.15
G12	7.90				6.11	2.34	2.59	4.64	4.14

[a] 0.1 M NaCl, 10 mM phosphate, H_2O, pH 6.35, 5 °C; exchangeable protons. [b] 0.1 M NaCl, 10 mM phosphate, D_2O, pH 6.35, 25 °C; nonexchangeable protons.

Table III: Proton Chemical Shifts in the G·C 12-mer Duplex

	chemical shifts (ppm)[a]						
base pair	T-H3	G-H1	C-H4b	C-H4e	A-H6b	A-H6e	A-H2
C1·G12		13.13	8.15	7.02			
G2·C11		13.05	8.44	6.63			
C3·G10		12.92	8.37	6.49			
G4·C9		12.85	8.53	6.99			
A5·T8	13.84				7.75	5.86	7.64
G6·C7		12.83	7.94	6.46			

	chemical shifts (ppm)[b]								
base	H8	H2	H6	H5/CH3	H1′	H2′	H2″	H3′	H4′
C1			7.63	5.89	5.76	1.96	2.41	4.70	4.07
G2	7.97				5.91	2.67	2.74	4.96	4.36
C3			7.30	5.39	5.67	1.90	2.32	4.84	4.16
G4	7.88				5.42	2.66	2.75	5.00	4.31
A5	8.07	7.65			6.09	2.66	2.91	5.06	4.43
G6	7.61				5.70	2.51	2.59	4.95	4.37
C7			7.33	5.18	5.84	2.03	2.49	4.65	4.20
T8			7.45	1.56	6.08	2.17	2.52	4.88	4.21
C9			7.50	5.67	5.61	2.11	2.41	4.86	4.13
G10	7.92				5.87	2.64	2.71	4.99	4.37
C11			7.33	5.45	5.78	1.90	2.33	4.82	4.15
G12	7.93				6.15	2.38	2.62	4.67	4.18

[a] 0.1 M NaCl, 10 mM phosphate, H_2O, pH 6.4, 5 °C; exchangeable protons. [b] 0.1 M NaCl, 10 mM phosphate, D_2O, pH 6.40, 25 °C; nonexchangeable protons.

expanded regions establishes the assignment of the sugar ring protons. The nonexchangeable base and sugar proton chemical shifts in the O⁶etG·C 12-mer at 25 °C, pH 6.90, are listed in the lower part of Table I. The corresponding nonexchangeable base and sugar proton assignments for the O⁶meG·C 12-mer and G·C 12-mer are listed in the lower parts of Tables II and III, respectively.

The CH_3 (1.11 ppm) and CH_2 (3.76 ppm) protons of the $O^6CH_2CH_3$ group exhibit NOEs between themselves in the nonexchangeable NOESY spectra (250-ms mixing time) of the O⁶etG·C 12-mer duplex at 25 °C and pH 6.90, as shown in the one-dimensional slices taken through these protons (panels A and B of Figure 8, respectively). The CH_3 protons of the O⁶etG4 exhibits NOEs to the CH_3 protons of the flanking T8 residue on the opposite strand and to the H5 and H6 protons of the 5′-flanking C3 residue on the same strand (Figure 8A). The CH_2 protons of O⁶etG4 exhibit a weak NOE to the H5 proton of the 5′-flanking C3 residue on the same strand (Figure 8B).

A slice through the 3.43-ppm $O^{13}CH_3$ resonance in the phase-sensitive NOESY spectrum (mixing time 250 ms) of the O⁶meG·C 12-mer duplex in D_2O at 25 °C shows a strong NOE to the other 3.71-ppm $O^{13}CH_3$ resonances and NOEs to the H5 of the flanking C3 base on the same strand and to the CH_3 of the flanking T8 on the partner strand (Figure 8C).

Phosphorus Spectra. The 121.5-MHz phosphorus spectra of G·C 12-mer, O⁶meG·C 12-mer, and O⁶etG·C 12-mer recorded with Waltz proton decoupling are plotted in panels A–C of Figure 9, respectively. The phosphorus resonances in all three duplexes were assigned by analyzing the heteronuclear ^1H–^{31}P COSY experiment (Zagorski & Norman, 1989) as described below for the O⁶etG·C 12-mer duplex (Figure 10A). Each phosphorus was assigned via the correlations to the sugar H3′ protons, and any ambiguities were resolved by analyzing

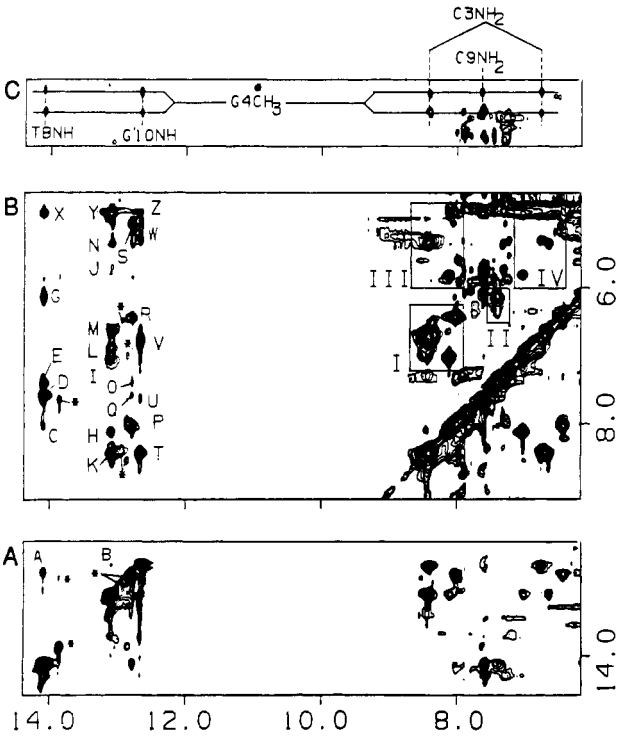

FIGURE 3: Expanded contour plots of the phase-sensitive NOESY spectrum (120-ms mixing time) of the O^{6}meG·C 12-mer duplex. Panels A–C cover the same expanded regions as in Figure 2. Cross-peaks A–Y are assigned as follows: The 14.01-ppm imino proton of T8 develops NOEs to the imino proton of G6 (peak A), to the hydrogen-bonded (peak C) amino proton of C7, to the H2 (peak D) and the hydrogen-bonded (peak E) and exposed (peak G) amino protons of A5, and to the hydrogen-bonded and exposed amino protons of C9 (peak D). The 13.03-ppm imino proton of G12 develops NOEs to the hydrogen-bonded (peak H) and exposed (peak I) and H5 (peak J) protons of C1. The 13.04-ppm imino proton of G2 develops NOEs to the imino proton of G10 (peak B), to the hydrogen-bonded (peak K) and exposed (peak M) amino and H5 (peak N) protons of C11, and to the hydrogen-bonded (peak K) and exposed (peak L) amino protons of C3. The 12.71-ppm imino proton of G6 exhibits NOEs to the hydrogen-bonded (peak P) and exposed (peak R) amino and H5 (peak S) protons of C7, and to the H2 (peak Q) and hydrogen-bonded amino proton of A5 (peak O). The 12.71-ppm imino proton of G10 develops NOEs to the hydrogen-bonded (peak T) and exposed (peak V) amino and H5 (peak W) protons of C3 and to the hydrogen-bonded and exposed amino protons of C9 (peak U). Cross-peaks X–Z are chemical-exchange cross-peaks between the solvent H_2O and the imino protons of T8, G12, G2, and G10. Boxed regions I and II outline the NOE cross-peaks between the hydrogen-bonded and exposed cytosine and adenine amino protons, respectively. Boxed regions III and IV outline the NOE cross-peaks between the cytosine H5 protons and the hydrogen-bonded and exposed amino protons within the same base pair. The weak peaks labeled with asterisks are due to the minor component of the G·C 12-mer duplex in the O^{6}meG·C 12-mer duplex sample arising from spontaneous demethylation.

the relay cross-peaks to the H1′, H2′,2″, and H4′ protons. This is demonstrated in the slice through the most downfield resonance (assigned to T8-C9) at −3.87 ppm as shown in Figure 10B. The proton–phosphorus cross-peak assignments for the d(C3-*G4-A5)·(T8-C9-G10) hexanucleotide fragment in all three duplexes are listed in Table IV, while the complete phosphorus resonance assignments are given in Table V.

The phosphorus resonances in the G·C 12-mer, O^{6}meG·C 12-mer, and O^{6}etG·C 12-mer duplexes all lie within the spectral range (−3.9 to −4.5 ppm) typical of phosphodiester resonances in regular right-handed DNA except for a resonance in the O^{6}etG·C 12-mer duplex at −3.87 ppm (assigned to the T8-C9 phosphodiester), a resonance in the G·C 12-mer duplex at −4.62 ppm (assigned to C7-T8 phosphodiester), and

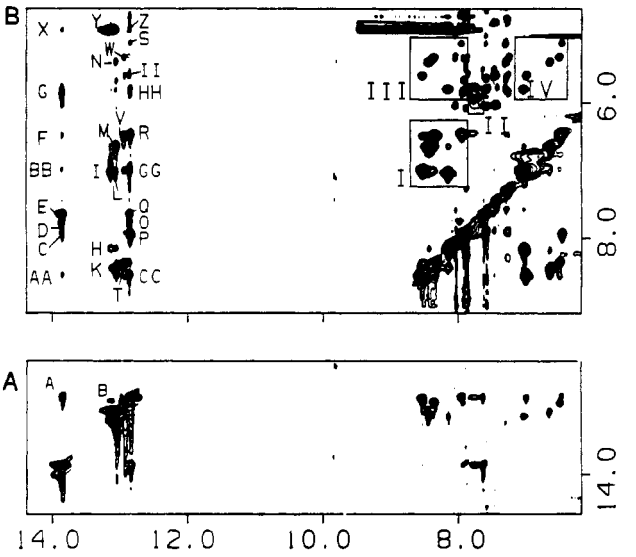

FIGURE 4: Expanded contour plots of the phase-sensitive NOESY spectrum (120-ms mixing time) of the G·C 12-mer duplex. Panels A and B are the same expanded regions as in Figure 2. Cross-peaks A–II are assigned as follows: The 13.84-ppm imino proton of T8 develops NOEs to the imino proton of G6 (peak A), to the hydrogen-bonded (peak C) amino proton of C7, to the H2 (peak E) and hydrogen-bonded (peak D) and exposed (peak G) amino protons of A5, and to the hydrogen-bonded (peak AA) and exposed (peak BB) amino protons of C9. The 13.13-ppm imino proton of G12 develops NOEs to the hydrogen-bonded (peak H) and exposed (peak I) protons of C1. The 13.05-ppm imino proton of G2 develops NOEs to the imino proton of G10 (peak B), to the hydrogen-bonded (peak K) and exposed (peak M) amino and H5 (peak N) protons of C11, and to the hydrogen-bonded (peak H) and exposed (peak L) amino protons of C1. The 12.83-ppm imino proton of G6 exhibits NOEs to the hydrogen-bonded (peak P) and exposed (peak R) amino and H5 (peak S) protons of C7 and to the H2 (peak Q) and hydrogen-bonded (peak O) and exposed (peak HH) amino protons of A5. The 12.92-ppm imino proton of G10 develops NOEs to the hydrogen-bonded (peak T) and exposed (peak V) amino and H5 (peak W) protons of C3. The 12.85-ppm imino proton of G4 develops NOEs to the hydrogen-bonded (peak CC) and exposed (peak GG) amino and H5 (peak II) protons of C9 and to the hydrogen-bonded (peak O) and exposed (peak HH) amino protons of A5. Cross-peaks X–Z are chemical-exchange cross-peaks between the solvent H_2O and the imino protons of T8, G12, G2, and G10. Boxed regions I and II outline the NOE cross-peaks between the hydrogen-bonded and exposed cytosine and adenine protons, respectively. Boxed regions III and IV outline the NOE cross-peaks between the cytosine H5 protons and the hydrogen-bonded and exposed amino protons within the same base pair.

several weak broad resonances due to the minor form (presumably a hairpin) present in these samples.

Discussion

Structure of DNA Duplexes. The G·C 12-mer, O^{6}meG·C 12-mer, and O^{6}etG·C 12-mer duplexes adopt right-handed helical conformations in solution with all the bases stacked into the helix with the normal anti-glycosidic torsion angle.

The purine H8 and pyrimidine H6 base protons (7.2–8.0 ppm) exhibit NOEs to their own sugar H1′ proton and to the 5′-linked sugar H1′ proton (5.4–6.2 ppm) in all three sequences (Figures 5–7). Base protons in purine (3′–5′)pyrimidine and pyrimidine(3′–5′)pyrimidine steps exhibit directional NOEs characteristic of right-handed helices in all three sequences (peaks A–G, Figures 5–7). Adenine H2 protons in the O^{6}meG·C 12-mer (peak G, Figure 6A) and in the G·C 12-mer (peak G, Figure 7A) duplexes develop NOEs to sugar H1′ protons on the partner strands, indicative of right-handed helices. Several NOEs are observed between the protons of the O^{6}alkG4·C9 base pair and protons of flanking bases and sugars, demonstrating that the O^{6}alkG4 and C9 bases are

Table IV: ^{31}P–^{1}H Heteronuclear Correlations and ^{31}P Chemical Shifts in the O⁶etG·C, O⁶meG·C,[a] and G·C[a] 12-mer Duplexes at 25 °C

	chemical shifts (ppm)					
	P	H3′[b]	H4′[b]	H2′,2″[b]	H1′	H4′[c]
O⁶etG·C 12-mer						
C3-O⁶etG4	−3.97	4.75	4.12	2.66, 2.08	5.49	4.45
O⁶etG4-A5	−4.19	4.99				4.40
T8-C9	−3.87	4.86		2.24, 2.34	5.92	4.24
C9-G10	−4.45	4.95		2.23, 2.51	6.08	4.31
O⁶meG·C 12-mer						
C3-O⁶meG4	−4.08	4.75		1.63, 2.17	5.58	4.30
O⁶meG4-A5	−4.09	4.97	4.30	2.71		4.40
T8-C9	−3.97	4.84	4.13	2.23, 2.38	5.90	4.20
C9-G10	−4.40	4.83		2.14, 2.54	6.04	4.28
G·C 12-mer						
C3-G4	−4.08	4.82	4.18	1.90, 2.34	5.68	4.42
G4-A5	−4.15	5.02	4.33			4.45
T8-C9	−4.46	4.89				4.14
C9-G10	−3.95	4.90	4.14	2.13, 2.42	5.60	4.39

[a] Data not shown. [b] O3′-Linked ^{31}P–^{1}H correlations. [c] O5′-Linked ^{31}P–^{1}H correlations.

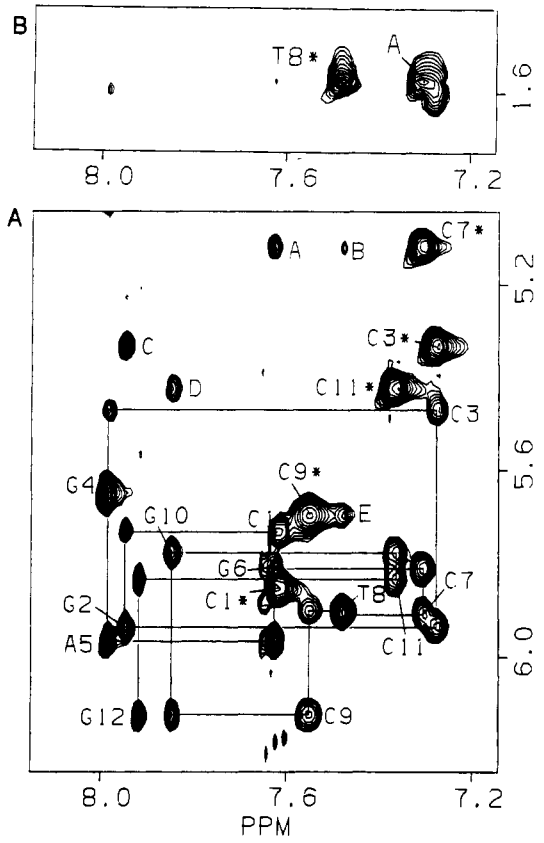

FIGURE 5: Expanded regions of the phase-sensitive NOESY spectrum (mixing time 250 ms) of the O⁶etG·C 12-mer duplex in 0.1 M NaCl, 10 mM phosphate, and D_2O, pH 6.35 at 25 °C. (A) Distance connectivities between the base protons (7.0–8.5 ppm) and the sugar H1′ protons (5.0–6.4 ppm). (B) Distance connectivities between the base protons (7.0–8.5 ppm) and the CH_3 protons (1.0–1.9 ppm). The cytosine H6–H5 and thymine H6–$CH_3$5 cross-peaks are designated by asterisks. The cross-peaks A–E are assigned as follows: (A) H8 of G6 to the H5 of C7; (B) H6 of T8 to the H5 of C7; (C) H8 of G2 to the H5 of C3; (D) H8 of G10 to the H5 of C11; (E) H6 of T8 to the H5 of C9. Cross-peak A in (B) is assigned to the NOE between the H6 of C7 and the CH_3 protons of T8. The lines follow connectivities between adjacent base protons and their intervening sugar H1′ protons in the O⁶etG·C 12-mer duplex.

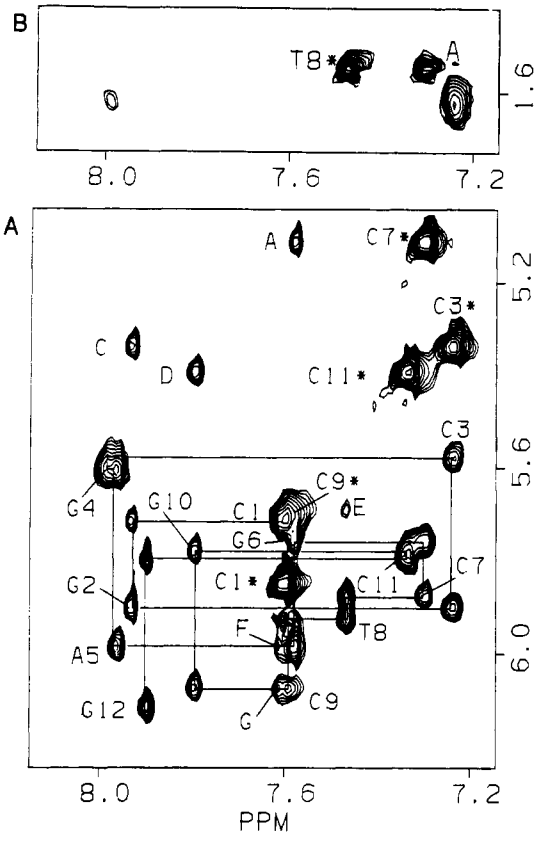

FIGURE 6: Expanded regions of the phase-sensitive NOESY spectrum (mixing time 250 ms) of the O⁶meG·C 12-mer duplex in 0.1 M NaCl, 10 mM phosphate and D_2O, pH 6.35 at 25 °C. (A) Distance connectivities between the base protons (7.0–8.5 ppm) and the sugar H1′ protons (5.0–6.4 ppm). (B) Distance connectivities between the base protons (7.0–8.5 ppm) and the CH_3 protons (1.0–1.9 ppm). The cytosine H6–H5 and thymine H6–$CH_3$5 cross-peaks are designated by asterisks. The cross-peaks A–E are assigned as in Figure 5, cross-peak F is assigned to the NOE between the H2 proton of A5 and the H1′ proton of A5, and cross-peak G is assigned to the NOE between the H2 proton of A5 and the H1′ proton of C9. The lines follow connectivities between adjacent base protons and their intervening sugar H1′ protons in the O⁶meG·C 12-mer duplex.

stacked into the helix in their respective duplexes.

In all three duplexes, every NOE from the purine H8 or cytosine H6 base proton to its own sugar H1′ proton is much weaker than the NOE between the cytosine H5 and H6 protons (Figures 5–7), indicating that every base maintains an anti conformation of the glycosidic torsion angle.

At 5 °C, five partially resolved imino protons are observed which resonate between 12.0 and 14.1 ppm in the O⁶meG·C 12-mer and O⁶etG·C 12-mer duplexes (panels B and C of Figure 1, respectively) and have been assigned from an analysis of the phase-sensitive NOESY spectra in H_2O (Figures 2 and 3). NOEs characteristic of Watson–Crick base pairing are detected between each of the thymine imino protons and the

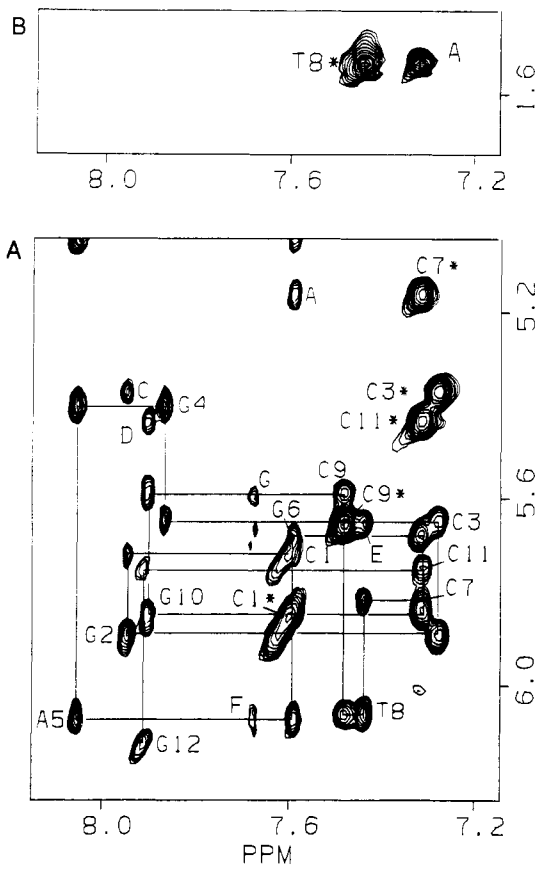

FIGURE 7: Expanded regions of the phase-sensitive NOESY spectrum (mixing time 250 ms) of the G·C 12-mer duplex in 0.1 M NaCl, 10 mM phosphate, and D_2O, pH 6.40 at 25 °C. (A) Distance connectivities between the base protons (7.0–8.5 ppm) and the sugar H1′ protons (5.0–6.4 ppm). (B) Distance connectivities between the base protons (7.0–8.5 ppm) and the CH_3 protons (1.0–1.9 ppm). The cytosine H6–H5 and thymine H6–$CH_3$5 cross-peaks are designated by asterisks. The cross-peaks A–E are assigned as in Figure 5, and cross-peaks F and G are assigned as in Figure 6. The lines follow connectivities between adjacent base protons and their intervening sugar H1′ protons in the G·C 12-mer duplex.

Table V: ^{31}P Chemical Shifts in the O^6etG·C 12-mer, O^6meG·C 12-mer, and G·C 12-mer Duplexes at 25 °C[a]

P	chemical shifts (ppm)		
	O^6etG·C	O^6meG·C	G·C
C1-G2	−4.16	−4.13	−4.17
G2-C3	−4.42	−4.35	−4.12
C3-*G4	−3.97	−4.08	−4.08
*G4-A5	−4.19	−4.09	−4.15
A5-G6	−4.07	−4.13	−4.37
G6-C7	−4.15	−4.03	−4.12
C7-T8	−4.47	−4.43	−4.62
T8-C9	−3.87	−3.97	−4.46
C9-G10	−4.45	−4.40	−3.95
G10-C11	−4.00	−4.03	−4.32
C11-G12	−4.02	−3.98	−4.05

[a] 0.1 M NaCl, 10 mM phosphate, pH ~6.4, D_2O.

H2 and amino protons of the A5·T8 base pair and between each of the guanine imino protons and the cytosine amino protons of the C1·G12, G2·C11, C3·G10, and G6·C7 base pairs in the O^6etG·C 12-mer and O^6meG·C 12-mer duplexes (Figures 2B and 3B, respectively). These data demonstrate that the C3·G10 and A5·T8 base pairs flanking the O^6alkG4·C9 modification site are intact and Watson–Crick base paired in solution.

The phosphorus chemical shifts of the O^6etG·C 12-mer and O^6meG·C 12-mer duplexes are very similar with only small differences in the range of 0.1 ppm centered at the O^6alkG4·C9

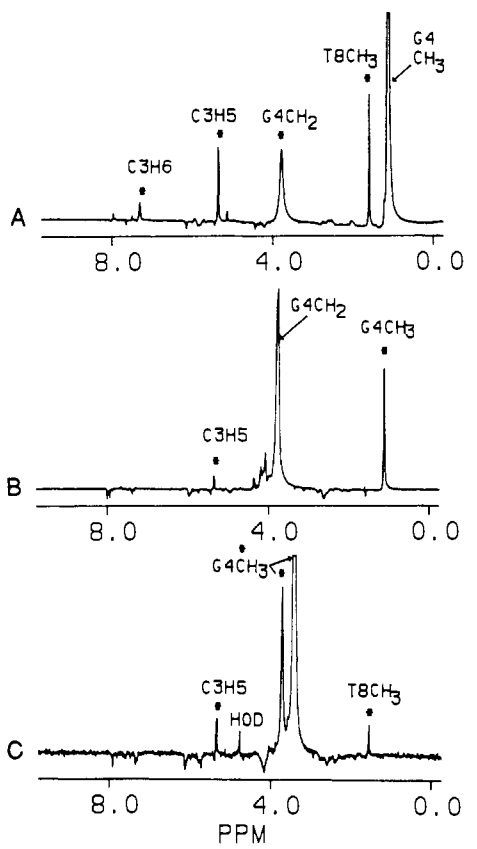

FIGURE 8: One-dimensional slices taken through (A) the CH_3 protons of O^6etG4 in the phase-sensitive NOESY spectrum (250-ms mixing time) of the O^6etG·C 12-mer duplex in D_2O, (B) the CH_2 protons of O^6etG4 in the phase-sensitive NOESY specrum (250-ms mixing time) of the O^6etG·C 12-mer duplex in D_2O, and (C) the CH_3 protons of O^6meG4 in the phase-sensitive NOESY spectrum (250-ms mixing time) of the O^6meG·C 12-mer duplex in D_2O. NOEs are designated by asterisks.

modification site (Figure 11A). However, large differences exist between the phosphorus spectrum of the O^6etG·C 12-mer and the G·C 12-mer. The difference is most pronounced in the T8-C9-G10 segment (Figure 11B), where the analogous chemical shifts of the O^6etG·C 12-mer and G·C 12-mer differ by more than 0.5 ppm. This indicates that O^6-alkylation of guanosine predominantly changes the backbone of the partner strand across from the lesion site.

O^6etG·C Base Pairing. The NOE data establish that the glycosidic torsion angles at the O^6etG4 and C9 residues are anti and that the O^6etG4 and C9 bases are stacked into the duplex. The structure of the base pair has been tentatively deduced from knowledge of the conformation of the alkyl group, the involvement of the amino group protons of C9 in hydrogen-bond formation, and from the alignment of the bases given by the intensity of the NOEs to the flanking base pairs. The chemical shifts of the proton and phosphorus resonances within the (C3-O^6alkG4-A5)·(T8-C9-G10) segment in the O^6meG·C 12-mer and O^6etG·C 12-mer duplexes are very similar (Table VI), indicating that the base pairs must have similar structure.

The pairing alignment of the bases at the O^6alkG4·C9 lesion site critically depends upon whether the *O^6*-alkyl group of O^6alkG4 is directed toward (syn relative to the N^1 of O^6alkG4) or away (anti relative to the N^1 of O^6alkG4) from C9 on the partner strand. Experimentally, NOEs are detected from the CH_3 group of O^6etG4 to the amino protons of C9, to the imino protons of T8 and G10, and to the CH_3 protons of T8 on the partner strand (Figures 3C and 8A), establishing a syn ori-

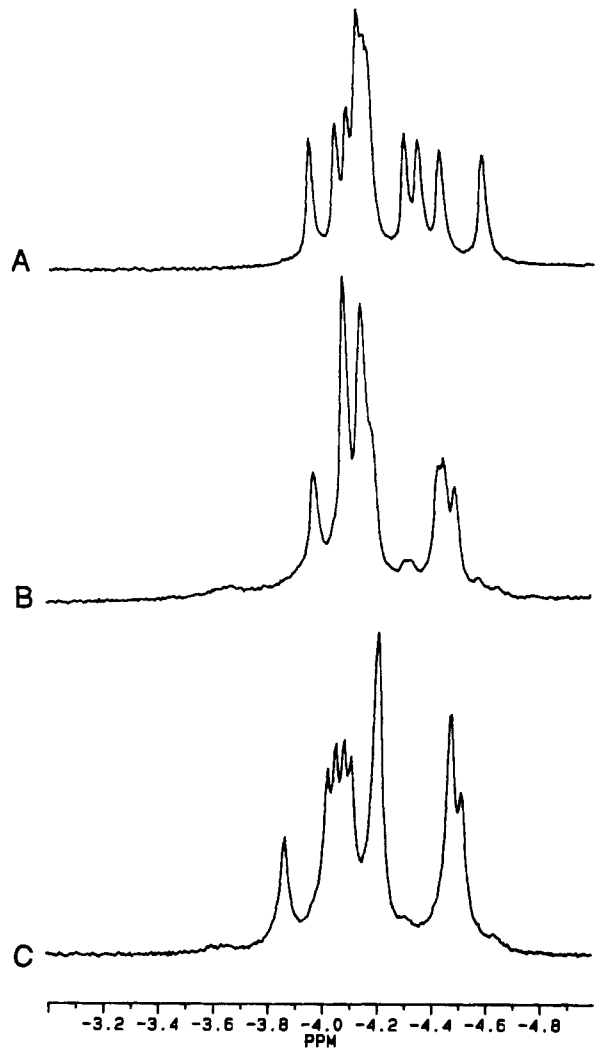

FIGURE 9: Proton Waltz decoupled 121.5-MHz phosphorus spectra (−3.0 to −5.5 ppm) of (A) the G·C 12-mer duplex in 0.1 M NaCl, 10 mM phosphate, and D_2O, pH 6.40 at 25 °C, (B) the O⁶meG·C 12-mer duplex in 0.1 M NaCl, 10 mM phosphate, and D_2O, pH 6.35 at 25 °C, and (C) the O⁶etG·C 12-mer duplex in 0.1 M NaCl, 10 mM phosphate, and D_2O, pH 6.40 at 25 °C.

entation of the *O*⁶-ethyl group in the O⁶etG·C 12-mer duplex. This conclusion is verified by the absence of an NOE between the CH_3 group and the H8 proton of O⁶etG4, which would indicate an anti orientation of the *O*⁶-ethyl group in the O⁶etG·C 12-mer duplex. The O^6CH_3 group of O⁶meG4 also adopts a syn orientation in the O⁶meG·C 12-mer duplex, since the O^6CH_3 group exhibits NOEs to the same protons on the partner strand T8-C9-G10 segment (Figures 3C and 8C) but not to its own H8 proton.

This syn conformation of the alkyl group is very important because the *O*⁶-alkyl group then acts as a spacer between the O⁶ atom of O⁶etG4 and the NH_2 group of C9, preventing hydrogen-bond formation between these atoms in the O⁶etG·C 12-mer duplex.

A previous NMR study of O⁶meG·C neither considered nor differentiated between the syn and anti orientations of the O^6CH_3 group, and the tentatively proposed pairing scheme was depicted with an anti orientation of the O^6CH_3 group at the O⁶meG·C lesion site (Patel et al., 1986).

A novel observation in the O⁶etG·C 12-mer was the detection of a broad exchangeable proton resonance at 7.78 ppm. An analogous resonance at 7.63 ppm was observed in the O⁶meG·C 12-mer. This exchangeable resonance has been assigned to the amino protons of C9. The observation of an

Table VI: Nonexchangeable Proton Chemical Shift Differences between the O⁶etG·C 12-mer Duplex and the O⁶meG·C 12-mer and G·C 12-mer Duplexes[a]

	Δδ (ppm)	
	O⁶etG·C/O⁶meG·C	O⁶etG·C/G·C
C3·G10		
G-H8	−0.05	0.08
C-H6	−0.05	0.03
C-H5	0.00	0.06
G-H1′	−0.06	0.10
C-H1′	0.10	0.20
*G4·C9		
G-H8	0.00	−0.10
C-H6	0.04	0.05
C-H5	0.00	−0.02
G-H1′	−0.05	−0.23
C-H1′	−0.05	−0.51
A5·T8		
A-H8	−0.02	0.08
A-H2	0.02	0.06
T-H6	−0.01	−0.03
T-CH_3	−0.03	−0.02
A-H1′	0.02	0.13
T-H1′	0.02	0.18

[a] 0.1 M NaCl, 10 mM phosphate, D_2O. The pH of the G·C 12-mer duplex was 6.40, the pH of the O⁶meG·C 12-mer duplex was 6.35, and the pH of the O⁶etG·C 12-mer duplex was 6.35.

Chart II

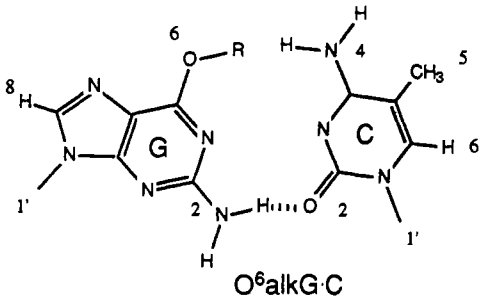

average single resoance, rather than the two distinct resonances, from the hydrogen-bonded and exposed amino protons, which is normally observed in G·C base pairs, is probably due to an increased rotation rate of the amino group about the C–NH_2 bond. This increased rate of rotation of the C9 amino group, observed in the O⁶etG4·C9 base pair, could be a consequence of the weakening of the hydrogen bond. This could result from either a change in the hydrogen-bond acceptor or an increase in the length of the hydrogen bond. The normal chemical shift range for cytosine amino protons involved in Watson–Crick base pairs is 8.0–8.5 ppm for the hydrogen-bonded amino proton and 6.4–7.0 ppm for the exposed amino proton. The amino protons of C9 in the control G·C 12-mer duplex have chemical shifts of 8.53 and 7.00 ppm for the hydrogen-bonded and exposed protons, respectively, giving an average value of 7.76 ppm. The amino protons of C9 in the O⁶etG·C 12-mer have a chemical shift of 7.78 ppm, reflecting rapid rotation around the C–NH_2 bond averaging the hydrogen-bonded and exposed amino proton chemical shift values.

The two possible pairing orientations corresponding to either Watson–Crick or wobble alignment of the O⁶etG4·C9 base pair are outlined in Charts II and III, respectively. The Watson–Crick alignment is stabilized by a single hydrogen bond in the minor groove with the O⁶ atom of O⁶etG4 and the NH_2 group of C9 spread apart by the ethyl group in the major groove (Chart II). The wobble alignment is stabilized by two amino–ring nitrogen hydrogen bonds with the ethyl group

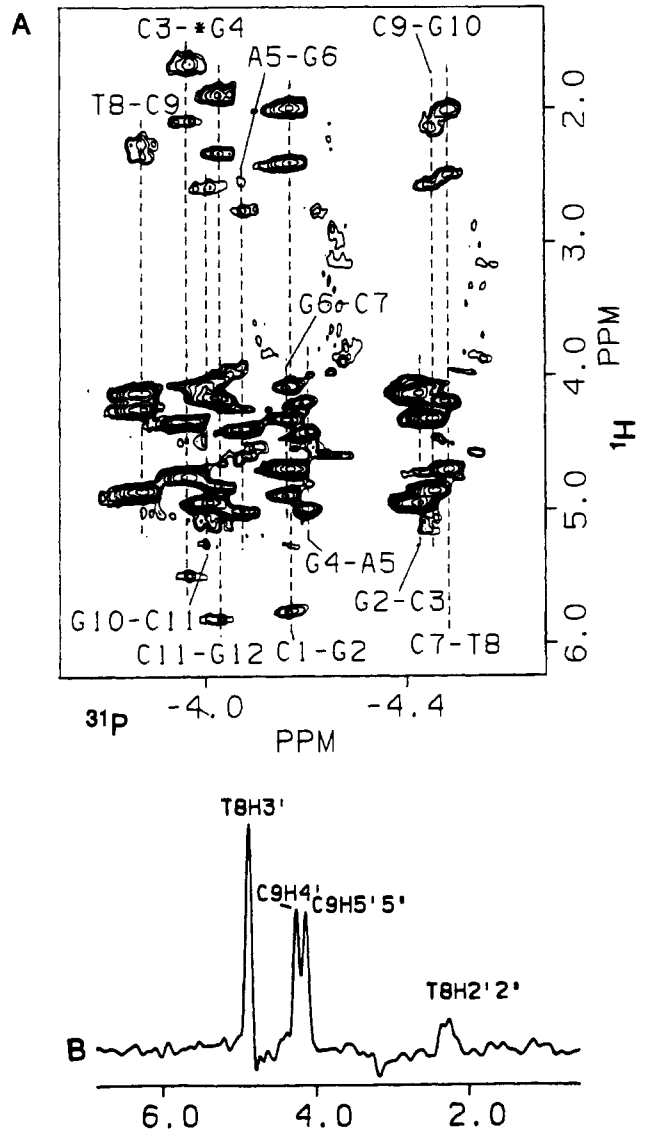

FIGURE 10: (A) Two-dimensional heteronuclear phosphorus (observe)–proton COSY contour plot of the O^{6}etG·C 12-mer duplex, D_2O solution at 25 °C. Note that only the positive contour levels are plotted for clarity, and the reference is to the positive contours. (B) One-dimensional slice taken through the most downfield phosphorus resonance (−3.87 ppm) corresponding to the T8-C9 phosphodiester group in the proton–phosphorus COSY in (A). Heteronuclear correlations to the O3′- and O5′-linked sugar protons are designated above the resonances.

Chart III

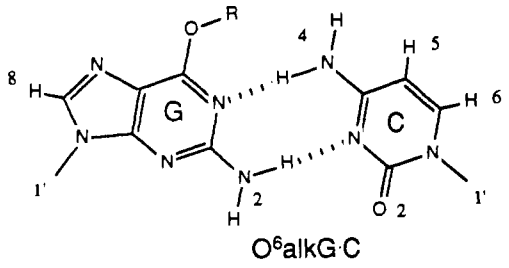

readily accommodated in the major groove (Chart III).

The amino protons of O^{6}etG4 could not be identified in the O^{6}etG·C 12-mer duplex because these protons are observed as a broad resonance due to an intermediate rotation rate around the C–NH_2 bond. The amino protons of C9 are hydrogen bonded in the wobble alignment (Chart III) but not in the Watson–Crick alignment (Chart II) of the O^{6}etG4·C9 base pair. The amino protons of C9 are observed as a single

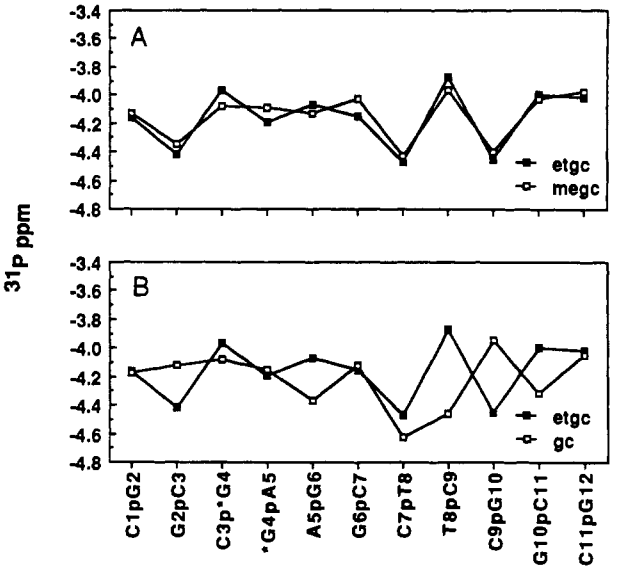

FIGURE 11: Graphical comparison of ^{31}P chemical shift as a function of phosphodiester position (A) between the O^{6}etG·C 12-mer duplex and the O^{6}meG·C 12-mer duplex and (B) between the O^{6}etG·C 12-mer duplex and the G·C 12-mer at 25 °C.

Chart IV

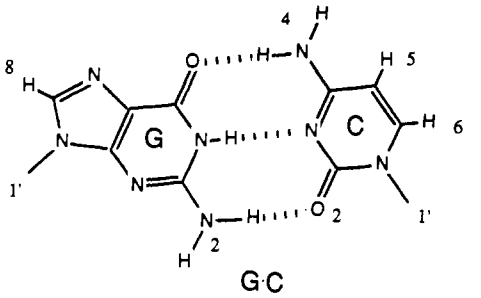

average resonance at 7.78 ppm, which is very similar to the average of the chemical shifts of the slowly rotating hydrogen-bonded and exposed amino protons of cytosines in Watson–Crick G·C base pairs. This observation is consistent with the wobble pairing outlined in Chart III, with the amino protons of C9 hydrogen bonded to the N^1 of O^{6}etG4 since the absence of hydrogen bonding would be reflected in a chemical shift upfield of the observed value of 7.78 ppm. For instance, the non-hydrogen-bonded amino protons of G4 resonate as an average resonance at 5.78 ppm in the G4·T9 mismatch in the G·T 12-mer duplex (Kalnik et al., 1989).

The observation of a single average resonance for the amino protons of C9 in the O^{6}etG4·C9 base pair rather than the separate hydrogen-bonded and exposed amino resonances normally observed for cytosines in Watson–Crick G·C base pairs may reflect the difference between the pairing of the amino protons of cytosine with the carbonyl oxygen in the G·C base pair (Chart IV) and the pairing of the amino protons of cytosine with the ring nitrogen in the proposed model of the O^{6}etG·C base pair (Chart III).

The NOEs observed from the CH_3 protons of O^{6}etG4 to the H5, H6, and amino protons of C3 and to the amino protons of A5 on the same strand and to the imino and CH_3 protons of T8, the amino protons of C9, and the imino proton of G10 on the partner strand (Figures 2 and 8) would be consistent with either the Watson–Crick (Chart II) or wobble (Chart III) alignments of the O^{6}etG4·C9 base pair. However, the amino protons of C9 would be displaced toward the helix axis in the wobble alignment (Chart III) and be stacked over the imino protons of the flanking C3·G10 and A5·T8 base pairs.

Table VII: Nonexchangeable Proton Chemical Shift Differences between the G·C 12-mer[a] and G·T 12-mer[b] Duplexes and between the O⁶etG·C 12-mer[a] and O⁶etG·T 12-mer[b] Duplexes

	Δδ (ppm)	
	G·C/G·T	O⁶etG·C/O⁶etG·T
C3·G10		
G-H8	−0.10	−0.15
C-H6	−0.15	−0.14
C-H5	−0.14	−0.16
G-H1′	−0.12	−0.12
C-H1′	−0.14	−0.05
*G4·C/T9		
*G4-H8	0.02	−0.04
C/T-H6	0.01	0.08
*G-H1′	−0.29	−0.22
C/T-H1′	−0.01	0.21
A5·T8		
A-H8	−0.03	0.01
A-H2	−0.10	−0.09
T-H6	−0.01	−0.02
T-CH_3	−0.06	−0.05
A-H1′	0.02	−0.03
T-H1′	−0.10	−0.26

[a] 0.1 M NaCl, 10 mM phosphate, D_2O, pH 6.0–6.4, 25 °C. [b] 1.1 M NaCl, 10 mM phosphate, D_2O, pH 6.2–6.4, 25 °C.

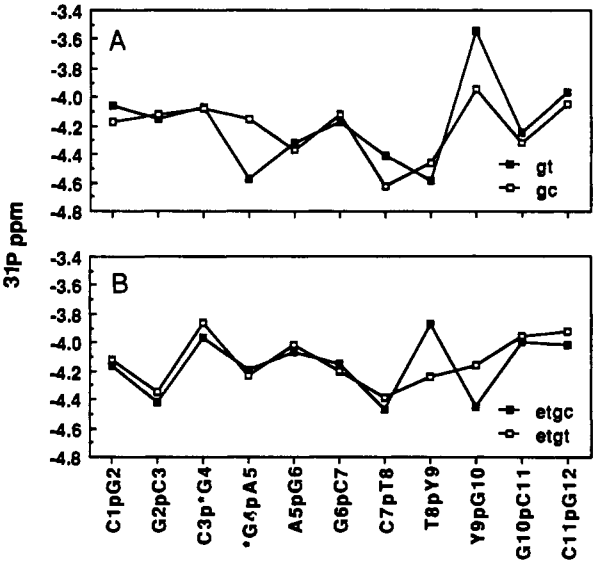

FIGURE 12: Graphical comparison of the ^{31}P chemical shift as a function of phosphodiester position (A) between the G·T 12-mer duplex and the G·C 12-mer duplex and (B) between the O⁶etG·C 12-mer duplex and the O⁶etG·T 12-mer duplex at 25 °C.

Thus, the observed NOEs between the amino protons of C9 and the imino protons of T8 (peak D, Figure 2B) and G10 (peak U, Figure 2B) are consistent with the proposed wobble O⁶etG·C pair (Chart III) in the O⁶etG·C 12-mer duplex.

Two planar alignments of the ethyl side chain exist for the syn orientation of the *O*⁶-ethyl group as drawn in Chart III of the preceding paper. These two orientations cannot be definitively differentiated, nor can a rapid interconversion between the two conformations be ruled out.

The change from the Watson–Crick G·C base pair (Chart IV) in the G·C 12-mer duplex to the proposed wobble O⁶etG·C base pair (Chart III) in the O⁶etG·C 12-mer duplex results in chemical shift differences at the imino protons (Tables I and III) and all of the sugar H1′ protons (Table IV) in the (C3-*G4-A5)·(T8-C9-G10) segment. The largest differences occur at the sugar H1′ protons of *G4 and C9, indicative of glycosidic torsion angle changes within the anti range between the G·C and O⁶etG·C base pairs.

Comparison of G·C and G·T Base Pairs. The switch from a Watson–Crick G·C pair in the G·C 12-mer duplex to the wobble G·T pair in the G·T 12-mer duplex results in specific changes in the proton and phosphorus spectra centered about the substitution site. The imino proton of G4 resonates at 12.85 ppm in the G4·C9 base pair and at 10.52 ppm in the G4·T9 base pair. This upfield shift reflects the change from an imino to ring-nitrogen hydrogen bond in a Watson–Crick base pair to an imino to carbonyl hydrogen bond in a wobble base pair. The 2-amino protons of G4 are too broad to detect in the G4·C9 pair but resonate as an average resonance at 5.78 ppm in the G4·T9 base pair. The guanine amino protons do not participate in hydrogen-bond formation in a wobble G·T base pair, which may account for their upfield shift and rapid rotation around the C–NH_2 bond. The imino and amino protons of the flanking C3·G10 and A5·T8 base pairs shift by 0.1–0.2 ppm in response to the substitution of the Watson–Crick G4·C9 pair (Table III) with the wobble G4·T9 pair [Table III of preceding paper (Kalnik et al., 1989)].

The base and sugar H1′ proton chemical shift differences between the G·C 12-mer and G·T 12-mer duplexes centered about the substitution site are listed in Table VII. The H5 and H6 protons of C3 shift downfield by 0.15 ppm on proceeding from the G·C 12-mer duplex to the G·T 12-mer duplex. These shifts most likely reflect the sliding of the G4 base toward the minor groove upon G4·T9 wobble pair formation, resulting in poorer overlap with the the major groove H5 and H6 protons of the adjacent C3 base in the G·T 12-mer duplex [Chart V of preceding paper (Kalnik et al., 1989)]. The sugar H1′ proton of G4 shifts downfield by 0.3 ppm, while the sugar H1′ of C/T9 is unperturbed on proceeding from the G4·C9 base pair to the G4·T9 base pair (Table VII). This suggests a greater perturbation at the glycosidic torsion angle of the G4 residue relative to the perturbation of the C/T9 torsion angle upon wobble G·T mismatch formation.

The sequence-dependent phosphorus chemical shifts in the G·C 12-mer and the G·T 12-mer duplexes are plotted in Figure 12A. The largest phosphorus chemical shift differences are detected O3′ to the substitution site with a 0.5-ppm upfield shift at the G4-A5 step and a 0.5-ppm downfield shift at the C/T9-G10 step on proceeding from the G·C 12-mer to the G·T 12-mer duplex.

Comparison of the O⁶etG·C and O⁶etG·T Base Pairs. The sugar H1′ protons within the T8-C/T9-G10 segment of the unmodified strand are perturbed to a greater extent than the sugar H1′ protons within the C3-O⁶etG4-A5 segment of the modified strand on proceeding from the O⁶etG·C 12-mer to the O⁶etG·T 12-mer duplex (Table VII). Similarly, the phosphorus resonances corresponding to the T8-C/T9 and C/T9-G10 steps on the unmodified strand exhibit the largest chemical shift differences between the O⁶etG·C 12-mer and O⁶etG·T 12-mer duplexes (Figure 12B). Thus, differences in the alignment between the proposed Watson–Crick O⁶etG4·T9 pair [Chart IV of preceding paper (Kalnik et al., 1989)] and the tentatively proposed wobble O⁶etG4·C9 pair (Chart III) primarily effect the glycosidic torsion angle and the backbone phosphate geometry in the T8-C/T9-G10 segment on the partner strand opposite the O⁶etG4 lesion site.

The CH_2 protons of O⁶etG4 exhibit distinctly different behavior in the O⁶etG·C 12-mer and the O⁶etG·T 12-mer duplexes. The CH_2 protons are nonequivalent (3.85 and 4.12 ppm) at the O⁶etG4·T9 lesion site [Figure 7A of preceding paper (Kalnik et al., 1989)], while a single resonance (3.76 ppm) characterizes the CH_2 protons at the O⁶etG4·C9 lesion site (Figure 8A). Restricted rotation about the O–CH_2 bond may account for the nonequivalence of the CH_2 protons of

O^6etG4 in the O^6etG·T 12-mer duplex. By contrast, the OCH_2CH_3 group of O^6etG4 does not interact with the NH_2 group of C9 in the tentatively proposed wobble alignment at the O^6etG4·C9 lesion site (Chart III). Thus the average resonance detected for the CH_2 protons is suggestive of free rotation around the O–CH_2 bond of O^6etG4 in the O^6etG·C 12-mer duplex.

Biological Implications. Alkylation at the O^6-position of guanine has profound effects on its base-pairing properties. The imino proton at N^1 is lost upon alkylation, and the bulky nature of the O^6-alkyl adduct prevents close contact on the major groove side of the bases and restricts the possible hydrogen-bonding orientations. This steric hindrance can be reduced in the O^6alkG·C base pair by a sliding of the cytosine base into the minor groove resulting in a wobble base pair, while in the O^6alkG·T base pair the steric hindrance is relieved by a spreading of the bases leading to a distorted Watson–Crick alignment with a widening of the major groove (Kalnik et al., 1989). This tentatively proposed sliding of the bases in the O^6alkG·C base pair allows two hydrogen bonds to form, whereas in the O^6alkG·T base pair only one strong hydrogen bond is intact. These proposed base-pairing schemes are consistent with the thermodynamic studies of Gaffney et al. (1984), which report that a dodecanucleotide duplex containing an O^6meG·C base pair is more stable than the same dodecanucleotide duplex containing an O^6meG·T base pair. Thus, characteristics other than the hydrogen-bonding properties of the O^6alkG residue are responsible for the miscoding observed in vitro and in vivo, where during the replication of DNA, O^6alkG in the template strand leads to the incorporation of thymine in the daughter strand (Gerchman & Ludlum, 1973; Abbot & Saffhill, 1979; Hall & Saffhill, 1983; Santos et al., 1983; Toorchen & Topal, 1983; Snow et al., 1984a,b; Green et al., 1984; Loechler et al., 1984). This preferential pairing may be determined by the requirement that the base pair within the active site of the DNA polymerase maintains a Watson–Crick alignment prior to daughter strand elongation, preventing cytosine from being incorporated opposite O^6alkG. The proofreading $3' \rightarrow 5'$ exonuclease activity may also selectively remove cytosine incorporated opposite O^6alkG (Kornberg, 1988). The recognition of the alkylated lesion by enzymatic repair systems may also depend on the alignment of the bases. Mismatch repair systems may recognize the wobble alignment of the bases in the O^6alkG·C lesion, which is the only lesion present after O^6-alkylation of native DNA prior to replication.

These results are also in agreement with NMR solution studies on O^4meT (Kalnik et al., 1988a,b), which demonstrate that the preferential base pairing of G rather than A with O^4meT is not due to the hydrogen-bonding patterns of these base pairs. The O^4meT base pair has a single hydrogen bond when paired with G and two wobble hydrogen bonds when paired with A at pH 5.5. DNA replication has historically been dominated by the central importance of hydrogen bonding of Watson–Crick and abnormal base pairs. These studies imply that the hydrogen bonding of the bases during replication is not the only information required in selecting the base to be incorporated into the daughter strand.

Registry No. G·C 12-mer, 121074-00-8; O^6meG·C 12-mer, 114317-50-9; O^6etG·C 12-mer, 114317-51-0.

References

Abbott, P. J., & Saffhill, R. (1979) *Biochim. Biophys. Acta 562*, 51–61.

Coulondre, C., & Miller, J.(1977) *J. Mol. Biol. 117*, 577–606.

Gaffney, B. L., Marky, L. A., & Jones, R. A. (1984) *Biochemistry 23*, 5686–5691.

Gerchman, L. L., & Ludlum, D. B. (1973) *Biochim. Biophys. Acta 308*, 310–316.

Green, C. L., Loechler, E. L., Fowler, K. W., & Essigman, J. M. (1984) *Proc. Natl. Acad. Sci. U.S.A. 81*, 13–17.

Hall, J. A., & Saffhill, R. (1983) *Nucleic Acids Res. 11*, 4185–4193.

Kalnik, M. W., Kouchakdjian, M., Li, B. F. L., Swann, P. F., & Patel, D. J. (1988a) *Biochemistry 27*, 108–115.

Kalnik, M. W., Kouchakdjian, M., Li, B. F. L., Swann, P. F., & Patel, D. J. (1988b) *Biochemistry 27*, 100–108.

Kalnik, M. W., Li, B. F. L., Swann, P. F., & Patel, D. J. (1989) *Biochemistry* (preceding paper in this issue).

Kornberg, A. (1988) *J. Biol. Chem. 263*, 1–4.

Lindahl, T. (1982) *Annu. Rev. Biochem. 51*, 61–87.

Loechler, E. L., Green, C. L., & Essigman, J. M. (1984) *Proc. Natl. Acad. Sci. U.S.A. 81*, 6271–6275.

Parthasarathy, R., & Fridey, S. M. (1986) *Carcinogenesis 7*, 221–227.

Patel, D. J., Shapiro, L., Kozolowski, S. A., Gaffney, B. L., & Jones, R. A. (1986) *Biochemistry 25*, 1036–1042.

Pegg, A. E. (1977) *Adv. Cancer Res. 25*, 195–269.

Pegg, A. E. (1983) *Reviews in Biochemical Toxicology* (Hodgson, E., Bend, J. R., & Philpot, R., Eds.) pp 83–133, Elsevier, New York.

Pegg, A. E. (1984) *Cancer Invest. 2*, 223–231.

Richardson, K. K., Richardson, F. C., Crosby, R. M., Swenberg, J. A., & Skopek, T. R. (1987) *Proc. Natl. Acad. Sci. U.S.A. 84*, 344–348.

Santos, E., Reddy, E. P., Pulciani, S., Feldman, R. J., & Barbacid, M. (1985) *Proc. Natl. Acad. Sci. U.S.A. 80*, 4679–4683.

Singer, B. (1979) *J. Natl. Cancer Inst. 62*, 1329–1339.

Singer, B. (1985) *Environ. Health Perspect. 62*, 41–48.

Snow, E. T., Foote, R. S., & Mitra, S. (1984a) *J. Biol. Chem. 259*, 8095–8100.

Snow, E. T., Foote, R. S., & Mitra, S. (1984b) *Biochemistry 23*, 4289–4294.

Toorchen, D., & Topal, M. D. (1983) *Carcinogenesis 4*, 1591–1597.

Yamagata, Y., Kohda, K., & Tomita, K. (1988) *Nucleic Acids Res. 16*, 9307–9321.

Zagorski, M. G., & Norman, D. G. (1989) *J. Magn. Reson.* (in press).

Zarbl, H., Sukumar, S., Arthur, A. V., Martin-Zanca, D., & Barbacid, M. (1985) *Nature 315*, 382–386.